$Co_{5/3}Nb_{1/3}BO_4$: a new cobalt oxyborate with a complex magnetic structure

N.V. Kazak[1*], N.A. Belskaya[2], E.M. Moshkina[1], L.N. Bezmaternykh[1], A.D. Vasiliev[1,3], J. Bartolome[4], A. Arauzo[4,5], D.A. Velikanov[1], S.Yu. Gavrilkin[6], M.V. Gorev[1,3], G.S. Patrin[1,3], and S.G. Ovchinnikov[1,3]

[1]Kirensky Institute of Physics, FRC SB RAS, Krasnoyarsk, Russia

[2]Reshetnev Siberian State University of Science and Technology, Krasnoyarsk, Russia

[3]Siberian Federal University, Krasnoyarsk, Russia

[4]Instituto de Nanociencia y Materiales de Aragón (INMA), CSIC-Universidad de Zaragoza and Departamento de Física de la Materia Condensada, 50009 Zaragoza, Spain

[5]Servicio de Medidas Físicas, Universidad de Zaragoza, Zaragoza, Spain

[6]P.N. Lebedev Physical Institute of RAS, 119991 Moscow, Russia

Corresponding author:

Dr. Natalia Kazak

Laboratory of Physics of Magnetic Phenomena

Kirensky Institute of Physics

Akademgorodok 50, bld. 38

Krasnoyarsk, 660036 Russia

+7(391)249-45-56

nat@iph.krasn.ru

keywords: warwickites, ferrimagnet

Needle-shape single crystals of $Co_{5/3}Nb_{1/3}BO_4$ warwickite were grown using the flux technique. X-ray diffraction measurements have revealed an orthorhombic structure (Sp. Gr. *Pbnm*) where the octahedral M1 site is occupied by a mixture of Co^{2+}/Nb^{5+} ions and the M2 site is exclusively filled by Co^{2+} ions. Using *dc* magnetization measurements it was established that the new material undergoes two magnetic transitions: an antiferromagnetic transition at T_{N1}=27 K and a ferrimagnetic one at T_{N2}=14 K, below which a hysteresis cycle opens. Both magnetic transitions are marked by anomalies in the specific heat. High magnetic anisotropy with *c*-axis as a hard magnetization direction was detected.

1. INTRODUCTION

The transition metal borates and oxyborates are important for applications, for example, for lithium-ion (LIBs) and sodium-ion (SIBs) batteries [1-5] and also for fundamental interest in the interplay between charge, orbital, spin, and lattice degrees of freedom. Iron borate, $FeBO_3$, with calcite structure has been studied intensively since 1972 when a spontaneous magnetic moment at room temperature and simultaneous transparency in the visible spectral range has been reported [6, 7]. At high pressure, this material undergoes a spin-state crossover accompanied by insulator-semiconductor electronic transition with a drastic drop of the optical absorption edge [8, 9]. Later, the iron oxyborates with warwickite (Fe_2BO_4) [10] and ludwigite (Fe_3BO_5) [11] structures have attracted large attention due to charge-ordering (CO). The Fe_2BO_4 shows an incommensurate charge order below T_{CO}=340 K, while dimer states were found in Fe_3BO_5 below T_{CO}=283 K. In both materials, the charge ordering is accompanied by the structural and electronic transitions as it was found employing polarized resonant X-ray diffraction, Mossbauer spectroscopy, neutron diffraction, and electrical resistivity measurements [12-15]. Besides, a cascade of magnetic transformations appearing when cooling down and associated with the antiferro- and ferrimagnetic orderings of the several magnetic subsystems has been extensively studied by experimental methods and theoretical calculations [16-19].

The electronic and magnetic phase diagrams of oxy-/borates are complicated and permanently being updated. They are not restricted to iron compounds but include other Me=3d metals. Under ambient pressure conditions several structure types, such as calcite ($Me^{3+}BO_3$), warwickite ($Me^{2+}Me^{3+}BO_4$), ludwigite ($Me_2^{2+}Me^{3+}BO_5$), norbergite ($Me_3^{3+}BO_6$), pyroborate ($Me_2^{2+}B_2O_5$), and kotoite ($Me_3^{2+}B_2O_6$), can be obtained within the ternary system $Me-B-O$:

$$\frac{1}{2}(2n\cdot MeO + m\cdot Me_2O_3 + p\cdot B_2O_3), \quad (1)$$

where parameters n, m, and p correspond to the amounts of di- and trivalent metal, and boron ions per formula unit, respectively. Hence, the resultant oxy-/borate $Me_n^{2+}Me_m^{3+}B_pO_{n+\frac{3}{2}(m+p)}$ could depend on its stoichiometry. One could expect that changing in *n, m,* and p parameters could lead to new magnetic materials that are structurally linked to the known Fe oxy-/borates and thereby might possess potentially interesting physical properties. By analogy with the family of iron oxy-/borates $Fe_n^{2+}Fe_m^{3+}B_pO_{n+\frac{3}{2}(m+p)}$, it was proposed that Me=Ti [20], V [21, 22], Mn [23-27], Co [26,27,28], Cr [21,29], Cu [30], and Ni [26] compounds could also form such families. Indeed, the newly-discovered orthoborate V_2BO_4 [31] supplement the mixed-valence warwickite family. This material was found to show several anomalies in the temperature range 135-260 K associated with the crystallographic symmetry change and the transition to ferrimagnetic state at ~ 35 K. The metaborate $Co_4B_6O_{13}$ [32] recently added to the divalent cobalt oxyborates was reported to have

an almost spinless ground state and a periodically undulating magnetization curve indicative of quantization of the total spin per spin tetrahedron. Figure 1 presents a phase diagram of known structural types of 3*d* oxy-/borates within the ternary system (1). The left panel corresponds to the divalent oxy-/borates (m=0), while the right one includes both trivalent and mixed-valence compounds ($m\neq0$). It is obvious that far from all 3*d* metals form the borate polymorphs. It is also seen that the borate family containing the trivalent cobalt is restricted to just the ludwigite type and no other stoichiometry containing Co^{3+} ion was reported up to now. We have been unsuccessful in the synthesis of the cobalt calcite and warwickite phases and, hence, the stability of these structures is still under question. On the other hand, the substitution of trivalent ion by the higher valence ion $m \cdot Me^{3+} = (m-1) \cdot Me^{2+} + Me^{m+2}$ makes it possible to obtain the samples with increasing concentration of ions of one own sort. The cobalt warwickites with tetravalent substitution $Co_{1.5}Me_{0.5}BO_4$ (Me=Ti^{4+}, Zr^{4+}) have been reported [33], but its physical properties were hitherto unknown. By going this way and careful choice of starting materials, we have synthesized a new oxyborate $Co_{5/3}Nb_{1/3}BO_4$, where the amount of Co^{2+} ions per formula unit is as large as 83%. The compound has been studied by a combination of single-crystal X-ray diffraction, *dc* magnetization, and specific heat measurements. The new oxyborate was found to crystallize in warwickite structure and exhibits intriguing magnetic behaviour that is not inherent in warwickites but has a strong resemblance to ludwigites, namely to Fe_3BO_5. The material undergoes two magnetic transitions: paramagnetic-antiferromagnetic at T_{N1}=27 K and antiferromagnetic-ferrimagnetic at T_{N2}=14 K. The clear signs of long-range magnetic order, manifesting both in the *dc* magnetization and specific heat measurements, make it a unique heterometallic oxyborate, which is in line with homometallic ones such as Mn_2BO_4 (T_N=23 K) [23], V_2BO_4 (T_N=35 K) [31], Fe_2BO_4 (T_N=150 K) [13], Co_3BO_5 (T_N=42 K) [18], and Fe_3BO_5 (T_{N1}=110 K, T_{N2}=70 K) [14]. Results demonstrate a parallelism between cobalt and iron borate families.

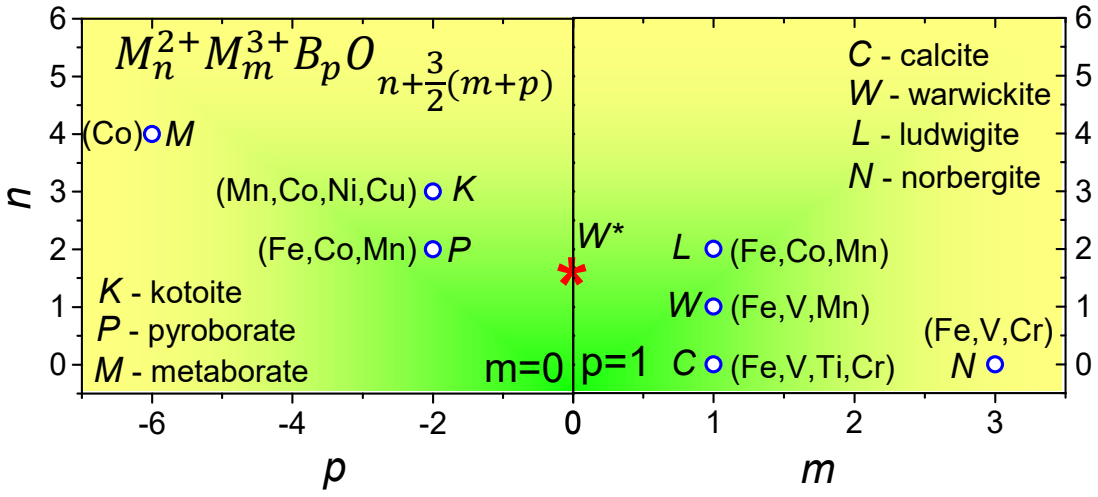

Fig. 1. The structural types diagram of transition metal oxy-/borates obtained within the ternary system M-B-O at ambient pressure. The parameters *n*, *m*, and *p* are amounts of di-, trivalent metal ions and boron per formula unit. Red star denotes a new $Co_{5/3}Nb_{1/3}BO_4$ warwickite.

2. EXPERIMENTAL TECHNIQUES

Single crystals of $Co_{5/3}Nb_{1/3}BO_4$ were grown using a flux method in the system $Bi_2Mo_3O_{12}$:3.63·B_2O_3:0.7·Na_2O:5.97 CoO:0.31 Nb_2O_5. The flux was prepared in a platinum crucible (V = 100 cm^3) at a temperature of 970 ºC by sequential melting of powders: first, $Bi_2Mo_3O_{12}$, B_2O_3, then Na_2CO_3 was added in portions, after that CoO and Nb_2O_5 were added in portions sequentially. The flux was homogenized at T = 1000ºC for 3 h, then the temperature was first rapidly reduced to 970 ºC and then slowly reduced at a rate of 4ºC/day. In two days, the crystal holder was extracted from the flux. The single crystals were separated by etching in a 20% aqueous solution of nitric acid.

Single crystals of $Co_{5/3}Nb_{1/3}BO_4$ warwickite have a pronounced needle shape up to 5 mm long. The cross-section shows a very well defined planar face, which allows to position the crystal according to direction 1 and 2 as shown below in Fig. 1S of Supplemental Material [34]. The cross-section has a size of 0.1 x 0.2 mm^2. The needle axis coincides with the *c*-axis of the crystal.

The X-ray diffraction patterns were collected from a single crystal at 296 K using the SMART APEX II single-crystal diffractometer (Bruker AXS) equipped with a PHOTON 2 CCD-detector, graphite monochromator, and Mo Kα radiation source. The structure was solved by direct methods [35] using the SHELXS program. The structure refinement was carried out by least-square minimization in the SHELXL program [36] using anisotropic thermal parameters of all atoms. The main information regarding crystal data, data collection, and refinement is reported in Table 1. The crystallographic data for the compound have been deposited with the Cambridge Crystallographic Data Centre, CCDC 2038293.

For magnetic measurements, one single crystal of 0.26 mg has been oriented and placed in the sample holder with the help of a microscope. The *dc* magnetization measurements were performed using a Quantum Design MPMS-XL. The sample was placed so that the needle axis was perpendicular (direction_1 and direction_2) and parallel (direction_3) to the external magnetic field (Fig. 1S [34]).

The specific heat measurements were performed on single crystalline samples with an overall mass of 2.2 mg in the temperature range of 2-200 K using a commercial instrument (Quantum Design PPMS).

3. RESULTS AND DISCUSSION

The crystal structure of $Co_{5/3}Nb_{1/3}BO_4$ was solved and the stoichiometry was confirmed. The compound was established to adopt the orthorhombic structure with *Pbnm* space group. The unit cell parameters are *a*=9.3336(7) Å, *b*=9.4039(7) Å, *c*=3.1793(2) Å, *V*=279.05(3) Å^3, and Z=8. The crystal structure has two crystallographically non-equivalent metal sites M1 and M2, which are octahedrally-coordinated (Fig. 2). The M1 site is occupied by Co and Nb ions with the ratio 0.66/0.34, while the M2 site is filled by Co ions (Table 2). By analyzing the M-O bond distances (Table 3) we established that both octahedra are compressed along the main axis with an average bond length <M1-O>=2.088(2) Å and <M2-O>=2.109(2) Å. The octahedral distortions were estimated through the main component of electric field gradient tensor V_{zz} similarly as it was done for other oxyborates [23, 37]. The distortion parameters are $V_{zz}(1)$=0.16 e/A^3 and $V_{zz}(2)$=0.08 e/A^3, for $M1O_6$ and $M2O_6$ octahedra, respectively. So, the $M1O_6$ octahedron is smaller and more distorted. Using a bond valence sums (BVS) [38] method the average oxidation states for Co ions occupying M1 and M2 sites were calculated to be +2.13 and +1.99, respectively. The same BVS analysis for Nb and B ions gives the value of +3.80 and +2.95, respectively. Thus, we conclude that the spacious M2 site is exclusively occupied by Co^{2+} ions. Taking into account the Nb ion distribution determined by single-crystal X-ray diffraction the oxidation state of M1 metal site was found to be +2.7, which is close to +3 expected from the general formula of the warwickite. This is in line with the conclusion that in warwickites the structure is only stable when the size of the divalent cation Me^{2+} at M2 site is larger than that one of the trivalent Me^{3+} at M1 site [39]. Although there is a large ionic-size mismatch between HS Co^{2+} (0.745 Å) and Nb^{5+} (0.64 Å), whereas ionic radius of LS Co^{2+} is 0.65 Å [40], we conjecture that Co^{2+} ions adopt a HS state. This conclusion is supported by its large abundance in oxyborates as compared to LS Co^{2+}, and the subsequent analysis of magnetic properties (see Table 5 and text below).

Table 1.Crystallographic data and main parameters of processing and refinement $Co_{5/3}Nb_{1/3}BO_4$.

Crystal data	
M_r	113.32
Space group, Z	P*bnm* (62), 8
Size, mm	0.27×0.07×0.05
T, K	296
a, (Å)	9.3336(7)
b, (Å)	9.4039(7)
c, (Å)	3.1793(2)
V, (Å^3)	279.05(3)
D_x, Mg/m^3	4.864
μ, mm^{-1}	11.063
Data collection	
Wavelength	MoK$_\alpha$, λ= 0.71073Å
Measured reflections	5484
Independent reflections	756
Reflections with I>2σ(I)	673
Absorption correction	Multiscan

R_{int}	0.0452
$2\theta_{max}$ (°)	71.92
h	-15 → 15
k	-15 → 15
l	-5 → 5
	Refinement
$R[F^2>2\sigma(F^2)]$	0.0307
$wR(F^2)$	0.0738
S	1.139
Weight	$w=1/[\sigma^2(F_o^2)+(0.0314P)^2+0.71P]$
Extinction	0.065(4)
$(\Delta/\sigma)_{max}$	0.00
$\Delta\rho_{max}$, e/Å^3	1.11
$\Delta\rho_{min}$, e/Å^3	-2.78

Table 2. Coordinates of atoms, occupancy and equivalent isotropic displacement parameters of $Co_{5/3}Nb_{1/3}BO_4$.

	x	y	z	Ueq	S.O.F.
Co1	0.07608(5)	0.11423(5)	0.2500	0.01571(14)	0.656(9)
Nb1	0.07608(5)	0.11422(5)	0.2500	0.01571(14)	0.344(9)
Co2	0.18185(5)	0.40016(4)	0.7500	0.01041(13)	
O1	0.2466(2)	0.2531(2)	0.2500	0.0107(4)	
O2	0.3847(3)	0.4875(3)	0.7500	0.0122(4)	
O3	0.0044(3)	0.2599(2)	0.7500	0.0129(4)	
O4	0.3626(4)	0.0295(3)	0.2500	0.0205(6)	
B	0.3718(4)	0.1739(4)	0.2500	0.0090(5)	

Table 3. Main bond lengths of $Co_{5/3}Nb_{1/3}BO_4$.

bond	distance (Å)	bond	distance (Å)	bond	distance (Å)
Co1|Nb1—O2^{i}	2.0201(15)	Co2—O4^{viii}	2.0440(17)	B—O3^{xi}	1.386(4)
Co1|Nb1—O2^{ii}	2.0201(15)	Co2—O4^{ix}	2.0440(17)	B—O4	1.361(4)
Co1|Nb1—O2^{iii}	2.027(3)	Co2—O2	2.064(2)	B—O1	1.386(4)
Co1|Nb1—O1	2.059(2)	Co2—O3	2.117(2)		
Co1|Nb1—O3^{iv}	2.2021(16)	Co2—O1	2.1917(16)		
Co1|Nb1—O3	2.2022(16)	Co2—O1^{vii}	2.1917(16)		

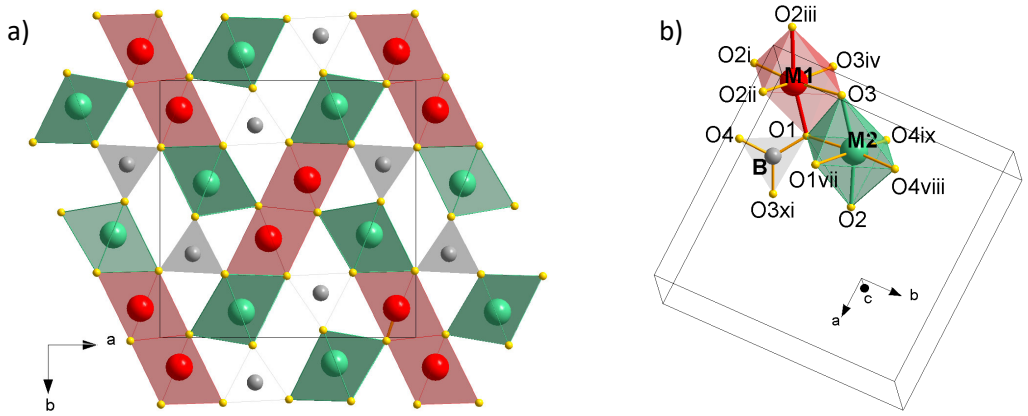

Fig. 2. a) The crystal stricture of new oxyborate projected in *ab*-plane. The non-equivalent metal sites M1 and M2 are highlighted by red and green, respectively. The BO_3 groups are depicted by grey triangles. b) Metal and boron coordinations. The main octahedral axes as shown by red and green for M1 and M2 sites, respectively.

We examined the magnetic properties of the new oxyborate by *dc* magnetization measurements. An external magnetic field was directed in *ab*-plane (*dir*_1 and *dir*_2) and along the *c*-axis (*dir*_3). Field-cooled (FC) and zero-field-cooled (ZFC) *dc* magnetizations measured as

a function of the temperature with an applied field of 600 Oe at different crystal orientations are shown in Fig. 3. First we want to note that the magnetization of $Co_{5/3}Nb_{1/3}BO_4$ demonstrates a high anisotropy. The magnetization along the *c*-axis is 100 times lower than those obtained for directions in the *ab*-plane, where the difference between magnetic moments measured in-plane is about 20%. This clearly indicates that the *c*-axis is a hard magnetization direction. Next, the magnetization measurements of $Co_{5/3}Nb_{1/3}BO_4$ reveal two magnetic transitions. As Fig.3 and its inset demonstrate, the maximum in the magnetization at T_{N1}=27 K evidences an antiferromagnetic transition. A broad susceptibility upturn below T_{N2}=14 K evidences spin canting or some other ferro- or ferrimagnetic transition. Below T_{N2}, FC magnetization steadily increases on cooling and the ZFC drops to zero, being peaklike. For *dir*_1, we have additionally measured the magnetization at 50 Oe, 5 kOe, and 50 kOe (Fig. 4). A close examination in a weak field reveals another one anomaly that looks like a broad maximum at 20 K, which is then hidden by the growing magnetic moment induced by a magnetic transition at T_{N2}. In fact, the transition at T_{N2} is so sharp that in the fields of 5 kOe and above this anomaly is not visible. The observed temperature dependence of the magnetization is not in accord with ordinary antiferromagnetism but reflects a complex ferrimagnetic ordering of Co^{2+} magnetic moments with the magnetic sublattices, which possess magnetizations non-equivalent in magnitude and temperature rate.

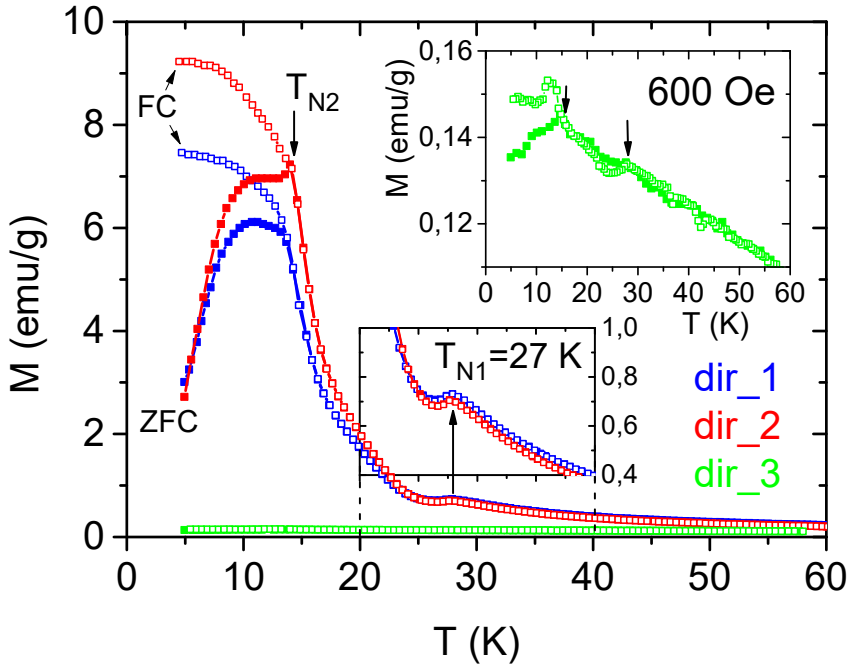

Fig. 3. Magnetization vs. temperature of $Co_{5/3}Nb_{1/3}BO_4$ single crystal at the field 600 Oe applied in *ab*-plane (dir_1, dir_2) and along *c*-axis (dir_3). The filled and empty symbols denote ZFC and FC regimes. Top inset shows strongly reduced magnetic moment along *c*-axis in zoom. Bottom inset is the enlarge plot of M(T) near magnetic transition at T_{N1}. Arrows show an onset of magnetic transitions.

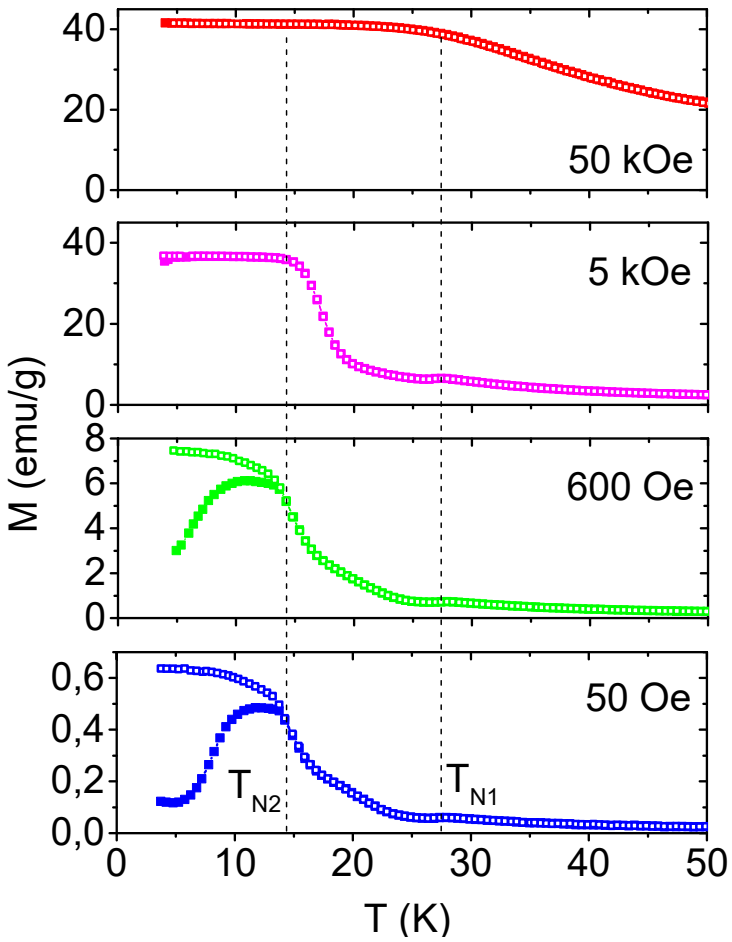

Fig. 4. The temperature dependencies of the magnetizations a $Co_{5/3}Nb_{1/3}BO_4$ single crystal measured at different fields applied in *ab*-plane (direction 1). The plot shows a sharp increase in magnetic moment below T_{N2}.

The average susceptibility $\chi_{av}(T) = \frac{\chi_{dir\_1}+\chi_{dir\_2}+\chi_{dir\_3}}{3}$, measured at H=50 kOe, follows above 100 K quite well the Curie-Weiss law (Fig. 5):

$$\chi(T) = \chi_0 + \frac{C}{T-\theta} \quad (2)$$

where χ_0 is the temperature independent term, C is the Curie-Weiss constant, and θ is the Curie-Weiss temperature. We note that for T>100 K, $M(H)$ is linear up to 50 kOe, so the susceptibility may be calculated as $\chi = M(H)/H$ at 50 kOe. The fits along the three directions and on the average susceptibility are given in Table 4. It is evidenced that the paramagnetic phase is highly anisotropic, with an *ab* easy plane anisotropy. Note, that the magnetic anisotropy observed in $Co_{5/3}Nb_{1/3}BO_4$ is the highest among those found in other warwickites Mn_2BO_4 [23] $Mn_{2-x}Mg_xBO_4$ [41], $Mn_{2-x}Fe_xBO_4$ [42], $Mg_{1-x}Co_xFeBO_4$ [43]. In fact, the anisotropy in $Co_{5/3}Nb_{1/3}BO_4$ is comparable with that we reported for Fe_3BO_5 and Co_3BO_5 ludwigites [18].

The constant χ_0=1.6·10^{-3} emu/mol and the parameter θ_{av}= -8.9 K were found. It is important to remark that the sign of the obtained θ in the individual fits is not indicative of the ferro or antiferro magnetic character of interactions along that direction, since this parameter includes an

anisotropic contribution (PRB 77, 064414 (2008)). The negative sign of θ_{av} points to an average antiferromagnetic exchange interactions between Co^{2+}. Most heterometallic warwickites studied up to now show high negative Curie-Weiss temperatures and rather low magnetic transition temperatures. For instance, θ was found to be -450 K ($NiFeBO_4$) [44], -315 K ($CoFeBO_4$) [43], and -283 K ($MgFeBO_4$) [43], while T_{SG}=12, 22, and 10 K, respectively. As a result, the majority of the warwickites of interest exhibit huge magnetic frustrations with empirical parameter $\eta=|\theta|/T_{SG}$ ranging from 8 to 37 [43]. We estimated the impact of the magnetic frustrations in $Co_{5/3}Nb_{1/3}BO_4$ through an average Curie-Weiss temperature θ_{av}, obtained using $\chi_{av}(T)$. One obtains $\eta=|\theta_{av}|/T_{N1}$=0.33 that indicates minoritary frustrations and is consistent with the onset of long-range magnetic order. Actually, the η value found for $Co_{5/3}Nb_{1/3}BO_4$ is the smallest among known warwickites including homometallic Fe_2BO_4 [13] and Mn_2BO_4 [23]. Therefore, this warwikite is different than those behaving as spin-glasses, while it resembles some Co containing ludwigites that show one or more long range order transitions. For example, in $Co_{3-x}Fe_xBO_5$, the compounds with x=0, 0.75 and 1 have θ's lower than T_c(T_{N2}) [18]. It can be expected for compounds exhibiting complicated magnetic sublattices and competing interactions, and in some cases giving rise to sequential magnetic transitions with different characters (ferro-, ferri-, or antiferromagnetic), as is the present $Co_{5/3}Nb_{1/3}BO_4$ warwikite.

Note that the average magnetic susceptibility in the field of 50 kOe is about χ_{av}(4.2 K) = $1.26\cdot10^{-1}$ emu/mol = $62\cdot10^{-5}$ emu/gOe which is one order higher than that reported for polycrystalline Fe_2BO_4 at similar conditions ($8.54\cdot10^{-5}$ emu/gOe) [13]. This behavior implies the enhancement of the ferrimagnetism in $Co_{5/3}Nb_{1/3}BO_4$, which is probably originated from the difference in the moduli and orientations of the magnetization sublattices.

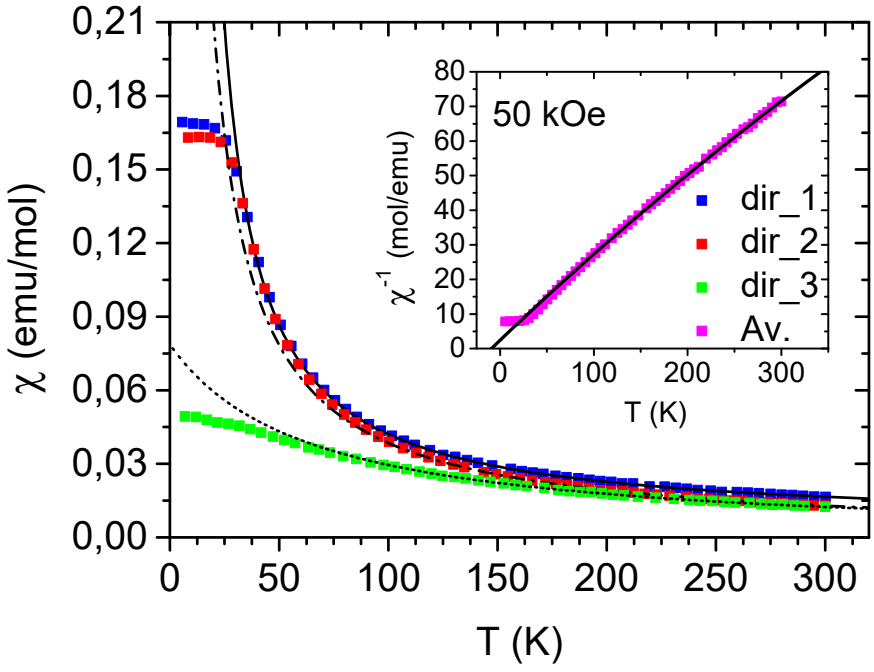

Fig. 5 Magnetic susceptibility for $Co_{5/3}Nb_{1/3}BO_4$ single crystal as a function of temperature in applied field of 50 kOe oriented in *ab*-plane (*dir*_1, and *dir*_2) and along *c*-axis (*dir*_3). The inset shows the inverse average susceptibility (Av.). The experimental data are shown by symbols, while dotted, dashed and solid lines denote fitting using *Eq*.1.

The average Curie-Weiss constant C_{av} =3.81 emu·K/mol corresponds to an effective magnetic moment μ_{eff}=5.52 μ_B/f.u. or 4.28 μ_B per Co^{2+} ion, while the value obtained for Co^{2+} ion (S = 3/2) for a spin-only magnetic moment with g=2 is 3.87 μ_B. One can conclude that in $Co_{5/3}Nb_{1/3}BO_4$ warwickite the Co^{2+} ions are a high-spin state and have a higher value of magnetic moment due to the orbital contribution, which is very typical for octahedrally coordinated Co^{2+}. Putting the effective magnetic moment of Co^{2+} ion $\mu_{eff}/Co = \sqrt{(g_{Co^{2+}})^2 \cdot S \cdot (S+1)}$, the obtained value of the effective magnetic moment corresponds to $g_{Co^{2+}}$=2.2, which is in accord with the usually observed value for Co^{2+} ion in octahedral coordination. Noteworthy, that value of μ_{eff} for $Co_{5/3}Nb_{1/3}BO_4$ is extremely close to that extracted in a similar way for Co_3BO_5 ludwigite, μ_{eff}=4.0 μ_B per Co^{2+} ion, where the Co^{2+} ions are assumed to be in a high-spin state, while the Co^{3+} ion is in a low-spin state. We also note that the experimentally observed value of μ_{eff} for $Co_{5/3}Nb_{1/3}BO_4$ is comparable to those found for other borate systems containing divalent cobalt (Table 5).

Table 4.Magnetic parameters of $Co_{5/3}Nb_{1/3}BO_4$ extracted in the paramagnetic phase.

	χ_0 (emu/mol)	C (emu·K/mol)	θ (K)	μ_{eff} (μ_B/f.u.)
dir_1	4.9 ± 0.1 ·10^{-3}	3.38± 0.02	8.7 ± 0.5	5.2 ± 0.1
dir_2	0.9 ± 0.1 ·10^{-3}	3.51 ± 0.02	7.8 ± 0.4	5.3 ± 0.1
dir_3	0.0 ± 0.5 ·10^{-3}	4.6 ± 0.2	-54 ± 6	6.1 ± 0.1
average	1.6± 0.2 ·10^{-3}	3.81 ± 0.08	-8.9 ± 2.4	5.52 ± 0.06

Table 5. The effective magnetic moments experimentally observed for different oxy-/borates containing divalent cobalt ions.

	$Co_{5/3}Nb_{1/3}BO_4$ [p.w.]	Co_3BO_5 [45]	$Co_2B_2O_5$ [27]	$Co_3B_2O_6$ [46]	$Co_4B_6O_{13}$ [32]	α-CoB_4O_7 [47]	$SrCo_2BPO_7$ [48]
μ_{eff} (μ_B/Co^{2+})	4.28	4.0*	4.96	4.92	4.90	5.00	5.00

* The effective magnetic moment is obtained assuming that Co^{2+} ions are in high-spin state, and Co^{3+} ions are in low-spin state.

To gain further insight into the magnetism of $Co_{5/3}Nb_{1/3}BO_4$, the isothermal magnetization curves were measured. Figure 6 shows $M(H)$ curves obtained for the applied magnetic field in *ab*-plane (*dir*_1). A hysteresis cycle at T=4.2 K is an intrinsic sign of a ferro- or ferrimagnetic state (Fig. 6a). The magnetization tends to the saturation at high fields. The saturation moment obtained by linear extrapolation of the high-field magnetization data to zero field yields M_s(4.2 K)=1.27 μ_B/f.u.. The remanent magnetization M_r=0.47 μ_B/f.u. is only 37% of the M_s. The coercive field

H_C(4.2 K)=1 kOe. As the compound is heated the magnetization curve is drastically modified. Although the M_s remains almost constant, the coercive field rapidly decreases down to 150 Oe at 10 K and becomes zero at 20 K (Fig. 6b,c). At the same temperature, which is in temperature range $T_{N2}<T<T_{N1}$, the magnetization curve shows zero magnetic remanence and a complex shape reflecting the magnetization process of the magnetic sublattices (Fig. 6c). Finally, at $T>T_{N1}$ the material exhibits a paramagnetic behavior (Fig. 6d).

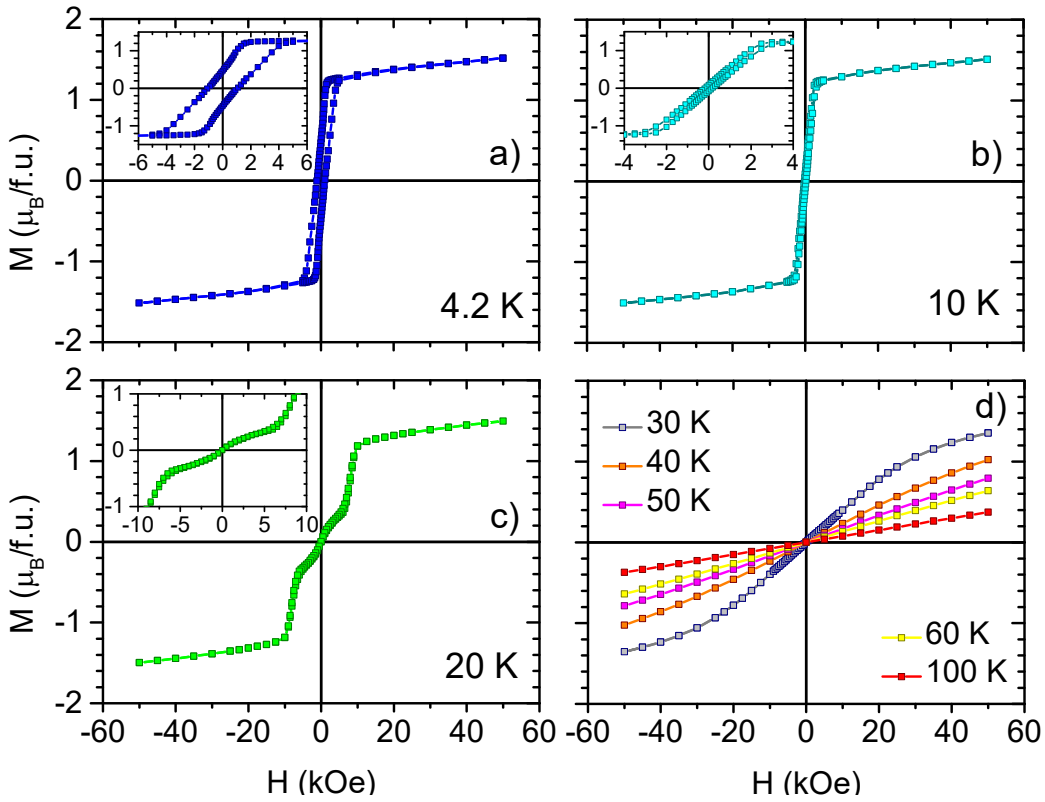

Fig. 6 Field dependences of the magnetization measured at temperature range of 4.2-100 K. The insets are low-field magnetization curves showing the transformation of the hysteresis loop upon heating.

The saturation magnetic moment as a function of temperature shows a monotonic decrease (Fig. 7a). Above T_{N1}=27 K, the non-zero M_s tail reflects short range correlations. The antiferromagnetic susceptibility $\chi_{AFM}(T)$ determined from the high-field slope of the $M(H)$ curves is typical for an antiferromagnet measured along the parallel direction (Fig. 7b). The first derivative of $\frac{d\chi_{AFM}(T)}{dT}$ has a maximum at the temperature corresponding to T_{N1}.

The saturation magnetic moment is rather small compared to that expected ~5 μ_B. The drastic reduction of the moment can be explained by the partial compensation due to a ferrimagnetic arrangement of Co moments. A naive accounting of the magnetization per formula unit for fully antiparallel spin arrangement yields of M_1=|-1.86| and M_2=3.13 μ_B for the simplest model of the two-sublattice ferrimagnet. Assuming that $M_{1,2} = n_{1,2}gS\mu_B$ are magnetic sublattices associated with crystallographically non-equivalent metal sites, S=3/2 is a spin value for Co^{2+}, and g=2 for

spin magnetism, the obtained concentrations of Co^{2+} ions at M_1 and M_2 sites equal $n_{1,2}$=0.62 and 1.04, respectively. These values are in good agreement with the site occupation factors obtained from single-crystal X-ray diffraction (Table 2). Thus, the presented data are consistent with a collinear order of the one up-spin and two-thirds down-spin d^7 ions (Co^{2+}), leading to a resultant magnetization of 1.27 μ_B/f.u..

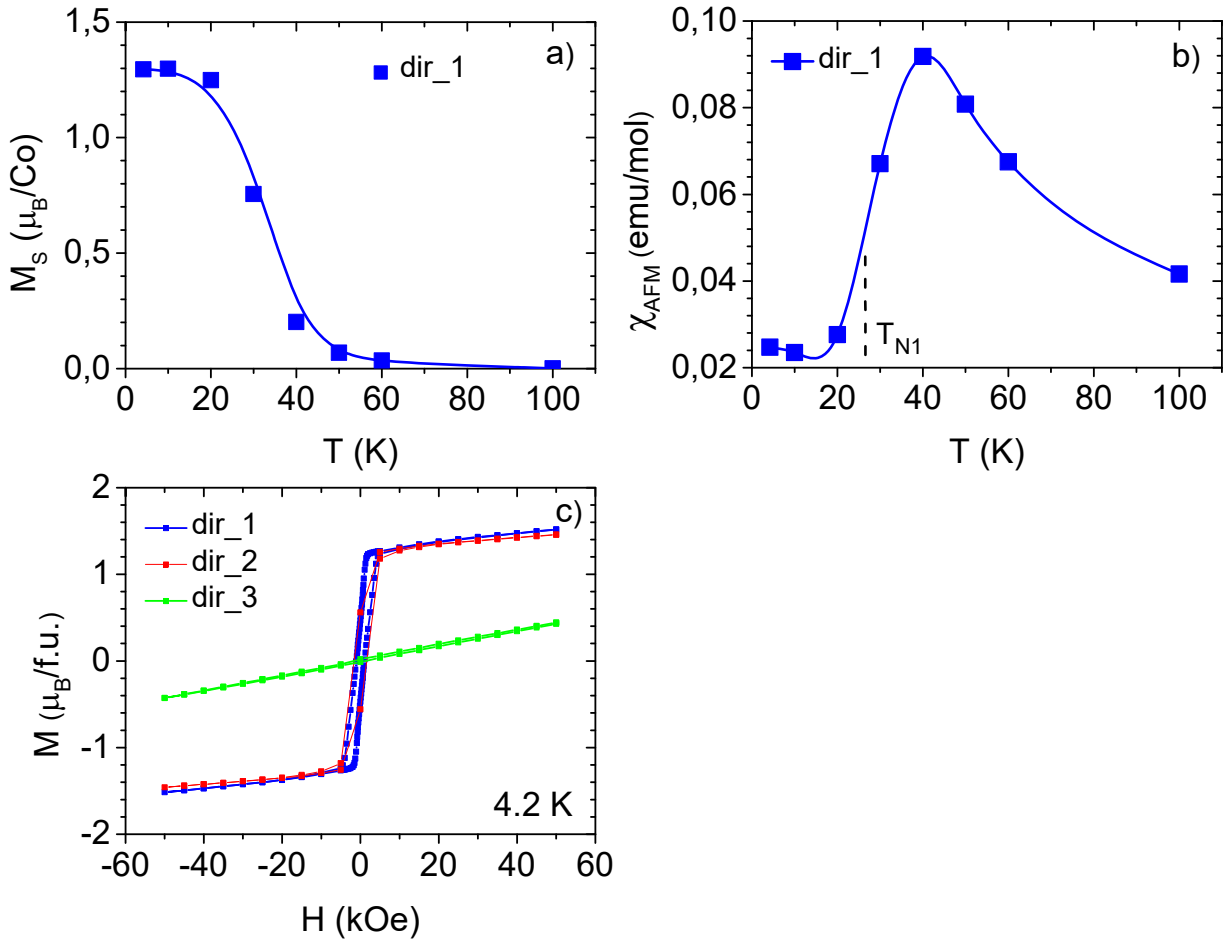

Fig. 7. a) The experimental saturation magnetic moment (μ_B/Co) *vs* temperature for $Co_{5/3}Nb_{1/3}BO_4$ (blue symbols); guide to the eye (solid curve). b) An antiferromagnetic susceptibility $\chi_{AFM}(T)$, determined from the high-field slope of the *M*(*H*) cycles (blue symbols). The dashed line corresponds to the maximum of the first derivative $\frac{d\chi_{AFM}(T)}{dT}$ showing the onset of antiferromagnetic ordering at T_{N1}=27 K. c) Hysteresis cycles at *T*=4.2 K for applied field in *ab*-plane and *c*-axis.

Additionally, the hysteresis cycles for the second direction of the magnetic field in *ab*-plane (*dir*_2) as well as along the *c*-axis (*dir*_3) were measured carefully (Fig. 7c), which confirm a high anisotropy of $Co_{5/3}Nb_{1/3}BO_4$ single crystal. In the *c*-direction the magnetization shows no hysteresis, with linear *M*(*H*) curves at all measured temperatures. The magnetization curves measured in *ab*-plane (*dir*_1 and *dir*_2) behave similar, without showing a noticeable difference in the magnitude.

The temperature-dependent measurements of specific heat C_p of $Co_{5/3}Nb_{1/3}BO_4$ have revealed two clear anomalies at T_{N1}=27 K and T_{N2}=14 K, which are in excellent agreement with the magnetization data (Fig. 8a). The anomaly at T_{N1} is a λ-type indicating a second-order phase transition, while the second one at T_{N2} has a broader shape. In the magnetic field, both anomalies smear out and are shifted to higher temperatures. At T=200 K, the specific heat C_p=100.7 J/mol K does not reach the thermodynamic limit $3Rz$=174.5 J/mol K of the lattice contribution, with R being the gas constant and z the number of ions per unit cell. The anomalous contribution of the specific heat ΔC_p was estimated using the Debye-Einstein approximation similar to the procedure applied for Mn_2BO_4 and Co_3BO_5 oxyborates [23, 45]. The temperatures far from anomalous regions were fitted. The Debye temperature was obtained to be Θ_D=356±20 K. This value is in good agreement with those of 512 K (Mn_2BO_4 [23]), 360 K (V_2BO_4 [31]), and 493 K (Co_3BO_5 [45]). The low-temperature part of the total entropy ΔS saturates at about 100 K, reaching approximately 10.1 J/mol K (Fig. 8b). The entropy released at magnetic transition amounts to $\Delta S(T_{N1})$=4.5±0.5 J/mol K that is about 42% of saturation value. This value (ΔS≈10 J/mol K) is very close to ΔS =9.6 J/mol K which corresponds to the transition being caused by the coupling of the ground Kramers doublets for the Co^{2+} ions, since the next excited doublet is at much higher energy and cannot be thermally populated, i.e. $\Delta S = R \cdot n_{Co^{2+}} \cdot ln\, 2$. Besides, the critical entropy can be compared to the value $\Delta S(T_N)$=8.30±1.6 J/mol K for Co_3BO_5 where two high-spin Co^{2+} ions are assumed to contribute to the entropy at the magnetic transition (Ref. [45] Kazak *et al.* to be published).

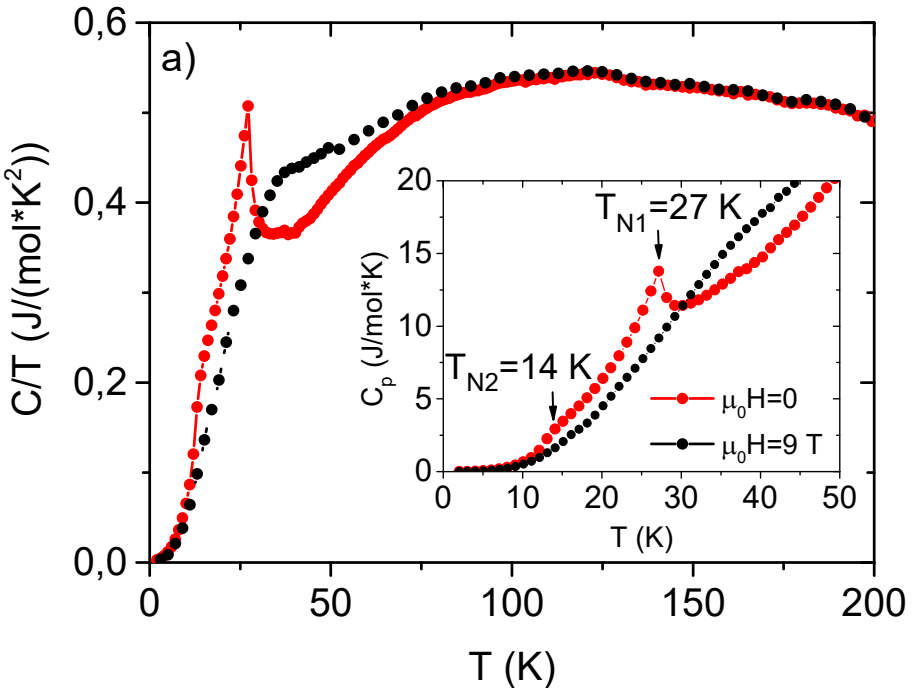

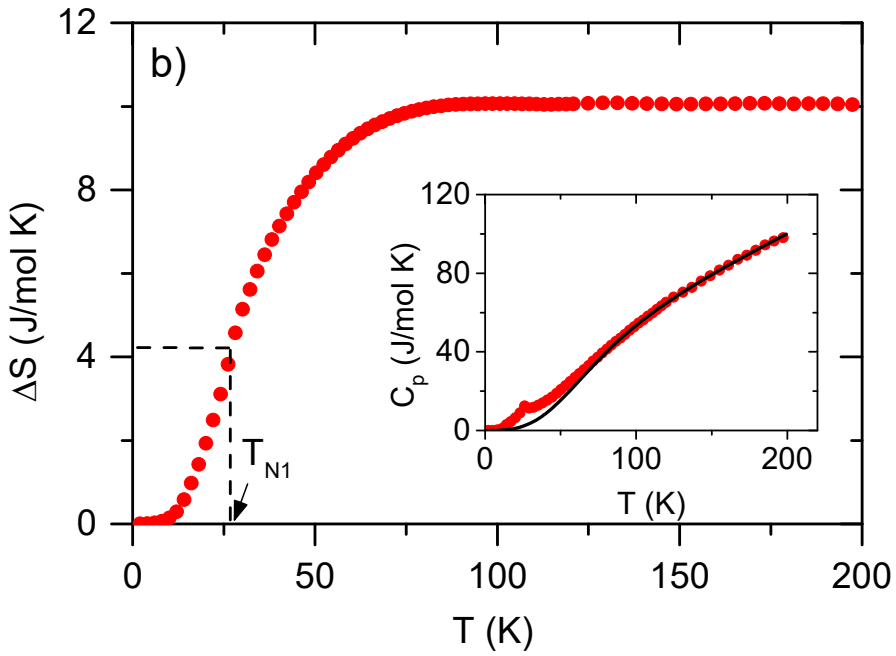

Fig. 8 a) Specific heat data for $Co_{5/3}Nb_{1/3}BO_4$ in C_p/T *vs* T representation measured under zero and 9 T applied fields. The inset: the temperature dependent C_p showing evidence of two anomalies associated with magnetic transitions at T_{N1} and T_{N2}. b) Entropy as a function of temperature. The dashed lines indicate the entropy released at magnetic transition T_{N1}. The inset shows experimental specific heat (red points) and the lattice contribution obtained by fitting to Debye-Einstein approximation.

So, we can conclude that the $Co_{5/3}Nb_{1/3}BO_4$ warwickite undergoes two magnetic transitions: the paramagnetic-antiferromagnetic at T_{N1}=27 K and antiferro-ferrimagnetic at T_{N2}=14 K. The abrupt growth in the *dc* magnetization below T_{N2} (in Fig. 3) correlates with this assumption. Neutron diffraction will be needed to confirm the spin orders below T_{N1} and T_{N2} transitions. Noteworthy is the strong similarity of the magnetic behavior of a new oxyborate with that of Fe and Co ludwigites. It is well known that Fe_3BO_5 exhibits two magnetic transitions: at T_{N1}=110 K the magnetic moments belonging to 4-2-4 triads are ordered antiferromagnetically along *a*-axis, while at T_{N2}=70 K magnetic moments of 3-1-3 triads are ordered ferrimagnetically along *b*-axis [14,18]. (Here, M1, M2, M3, and M4 are numbers of crystallographically non-equivalent metal sites in ludwigite structure). Unlike iron ludwigite, Co_3BO_5 demonstrates only one magnetic transition to the ferrimagnetic state at T_N=42 K, which is proposed to associated with the ordering of Co^{2+} magnetic moments belonging to M1, M2, and M3 sites whereas the Co^{3+} ions located at M4 site are assumed in a low-spin state [45]. The second transition becomes manifested if LS Co^{3+} ions are replaced by HS Fe^{3+} ions [49]. As a result, Co_2FeBO_5 shows two magnetic transitions similar to Fe ludwigite [14, 18]. In $Co_{5/3}Nb_{1/3}BO_4$ these two transitions although strongly shifted to the lower temperatures manifest themselves both in the magnetic and specific heat measurements indicating the common peculiarities of the magnetic ground state forming in warwickites and ludwigites.

4. CONCLUSIONS

By the changing in the stoichiometry of the oxy-/borates $Me_n^{2+}Me_m^{3+}B_pO_{n+\frac{3}{2}(m+p)}$ and using a pentavalent substitution, we have obtained a new cobalt compound $Co_{5/3}Nb_{1/3}BO_4$, in which the concentration of Co^{2+} ions per formula unit reaches 83%, contributing to the magnetism of the system. The single crystals were found to crystallize in the warwickite structure with space group *Pbnm*. The Co^{2+}/Nb^{5+} ions share the octahedral M1 site and the Co^{2+} ions fill exclusively the M2 site. The magnetic properties were studied through the *dc* magnetization measurements at applied fields along the crystallographic *c*-axis and in the *ab*-plane. New oxyborate was found to exhibit two magnetic transitions at T_{N1}=27 K and T_{N2}=14 K. First of them is associated with a long-range antiferromagnetic ordering of Co^{2+} magnetic moments, while the second has a ferrimagnetic origin. In the temperature range $T_{N2}<T<T_{N1}$ a magnetization curve shows a complex shape without any remanent magnetization. Below T_{N2} the hysteresis cycle is opened with the net moment 1.27 μ_B/f.u. originated from magnetic moments of different modulus and orientation. The *c*-axis was found to be a hard magnetization direction. The specific heat measurements were revealed two magnetic anomalies in accordance with magnetic measurements. The magnetic behavior of $Co_{5/3}Nb_{1/3}BO_4$ warwickite is straightly similar to that of ludwigites. It is evident, these materials have strong structural and magnetic affinities.

ACKNOWLEDGMENTS

The authors acknowledge M. Molokeev for the orientating the single crystal for magnetic measurements. The X-ray diffraction and specific heat measurements were carried out in the Common Access Facility Centres of SB RAS (Krasnoyarsk, Russia) and P.N. Lebedev Physical Institute of RAS (Moscow, Russia). This work has been financed by the Russian Foundation for Basic Research (project no. 20-02-00559). We acknowledge financial support from the Spanish MINECO DWARFS project MAT2017-83468-R and Gobierno de Aragón (Group, E12-20R).

REFERENCES

[1] H.F. Glass, Z. Liu, P.M. Bayley, E. Suard, S.H. Bo, P.G. Khalifah, ... & S.E. Dutton, MgxMn2–xB2O5 Pyroborates (2/3≤ x≤ 4/3): High Capacity and High Rate Cathodes for Li-Ion Batteries, Chem. Mat. 29(7) (2017) 3118-3125. https://doi.org/10.1021/acs.chemmater.7b00177

[2] H. Chen, B.B. Xu, Q.S. Ping, B.Z. Wu, X.K. Wu, Q.Q. Zhuang,... & B.F. Wang (2020). Co2B2O5 as an anode material with high capacity for sodium ion batteries. Rare Met. 39(9) (2020) 1045–1052. https://doi.org/10.1007/s12598-020-01383-8

[3] B. Xu, Y. Liu, J. Tian, X. Ma, Q. Ping, B. Wang, & Y. Xia, Ni3(BO3)2 as anode material with high capacity and excellent rate performance for sodium-ion batteries, Chem. Eng. J. 363 (2019) 285-291. https://doi.org/10.1016/j.cej.2019.01.089

[4] M. Dong, Q. Kuang, X. Zeng, L. Chen, J. Zhu, Q. Fan, ... & Y. Zhao, Mixed-metal borate FeVBO4 of tunnel structure: Synthesis and electrochemical properties in lithium and sodium ion batteries, J. Alloys Compd, 812 (2020) 152165. https://doi.org/10.1016/j.jallcom.2019.152165

[5] V. Pralong, B. Le Roux, S. Malo, A. Guesdon, F. Lainé, J.F. Colin, & C. Martin, Electrochemical activity in oxyborates toward lithium, J. Solid State Chem. 255 (2017) 167-171. https://doi.org/10.1016/j.jssc.2017.08.010

[6] I. Bernal, C. W. Struck, and J. G. White, New transition metal borates with the calcite structure, Acta Crystallogr. 16 (1963) 849-850. https://doi.org/10.1107/S0365110X63002255

[7] I.S. Edel'man, A.V. Malakhovskii, T.I. Vasil'eva, and V.N. Seleznev, Sov. Phys. Solid State 14 (1972) 2442.

[8] V.A. Sarkisyan, I.A. Troyan, I.S. Lyubutin, A.G. Gavrilyuk, and A.F. Kashuba, Magnetic collapse and the change of electronic structure of $FeBO_3$ antiferromagnet under high pressure, JETP Lett. 76 (2002) 664-669. https://doi.org/10.1134/1.1545580

[9] I.A. Troyan, M.I. Eremets, A.G. Gavrilyuk, I.S. Lyubutin, and V.A. Sarkisyan, Transport and optical properties of iron borate $FeBO_3$ under high pressures, JETP Lett. 78 (2003) 13-16. https://doi.org/10.1134/1.1609568

[10] J.P. Attfield, A.M.T. Bell, L.M. Rodriguez-Martinez, J.M. Greneche, R.J. Cernik, J.F. Clarke, D.A. Perkins, Electrostatically driven charge-ordering in Fe_2OBO_3, Nature 396 (1998) 655-658. https://doi.org/10.1038/25309

[11] M. Mir, R.B., Guimaraes, J.C. Fernandes, M.A. Continentino, A.C Doriguetto, Y.P. Mascarenhas, and L. Ghivelder, Structural Transition and Pair Formation in $Fe_3O_2BO_3$, Phys. Rev. Lett. 87 (2001) 147201. https://doi.org/10.1103/PhysRevLett.87.147201

[12] M. Angst, R.P. Hermann, W. Schweika, J.-W. Kim, P. Khalifah, H.J. Xiang, and D. Mandrus, Incommensurate Charge Order Phase in Fe_2OBO_3 due to Geometrical Frustration, Phys. Rev. Lett. 99 (2007) 256402. https://doi.org/10.1103/PhysRevLett.99.256402

[13] A.P. Douvalis, V. Papaefthymiou, A. Moukarika, T. Bakas, and G. Kallias, Mössbauer and magnetization studies of Fe_2BO_4, Journal of Physics: Condensed Matter 12 (2000) 177. https://doi.org/10.1088/0953-8984/12/2/307

[14] P. Bordet and E. Suard, Magnetic structure and charge ordering in Fe_3BO_5: A single-crystal x-ray and neutron powder diffraction study, Phys. Rev. B 79 (2009) 144408. https://doi.org/10.1103/PhysRevB.79.144408

[15] S.R. Bland, M. Angst, S. Adiga, V. Scagnoli, R.D. Johnson, J. Herrero-Martin, and P.D. Hatton, Symmetry and charge order in Fe_2OBO_3 studied through polarized resonant x-ray diffraction, Phys. Rev. B 82 (2010) 115110. https://doi.org/10.1103/PhysRevB.82.115110

[16] M. Matos, J. Terra, D.E. Ellis, and A.S. Pimentel, First principles calculation of magnetic order in a low-temperature phase of the iron ludwigite, J. Magn. Magn. Mater. 374 (2015) 148-152. https://doi.org/10.1016/j.jmmm.2014.08.025

[17] E. Vallejo and M. Avignon, Spin and charge ordering in three-leg ladders in oxyborates, Phys. Rev. Lett. 97 (2006) 217203. https://doi.org/10.1103/PhysRevLett.97.217203

[18] J. Bartolomé, A. Arauzo, N.V. Kazak, N.B. Ivanova, S.G. Ovchinnikov, Y.V. Knyazev, and I.S. Lyubutin, Uniaxial magnetic anisotropy in $Co_{2.25}Fe_{0.75}O_2BO_3$ compared to $Co_3O_2BO_3$ and $Fe_3O_2BO_3$ ludwigites, Phys. Rev. B 83 (2011) 144426. https://doi.org/10.1103/PhysRevB.83.144426

[19] I. Leonov, A.N. Yaresko, V.N. Antonov, J.P. Attfield and V.I Anisimov, Charge order in Fe_2OBO_3: An LSDA+ U study, Phys. Rev. B 72 (2005) 014407. https://doi.org/10.1103/PhysRevB.72.014407

[20] M. Huber and H.J. Deiseroth, Crystal structure of titanium (III) borate, $TiBO_3$, Zeitschrift fur Kristallographie 210 (1995) 685-685. https://doi.org/10.1524/zkri.1995.210.9.685

[21] T.A. Bither, C.G. Frederick, T.E. Gier, J.F. Weiher, and H.S. Young, Ferromagnetic VBO_3 and antiferromagnetic $CrBO_3$, Solid State Communications 8 (1970) 109-112. https://doi.org/10.1016/0038-1098(70)90582-X

[22] X. Zeng, Q. Kuang, Q. Fan, Y. Dong, Y. Zhao, S. Chen, and S. Liu, Synthesis, structure, and electrochemical performance of V_3BO_6 nanocomposite: A new vanadium borate as high-rate anode for Li-ion batteries, Electrochimica Acta 335 (2020) 135661. https://doi.org/10.1016/j.electacta.2020.135661

[23] N.V. Kazak, M.S. Platunov, Y.V. Knyazev, N.B. Ivanova, O.A. Bayukov, A.D. Vasiliev, and S.G. Ovchinnikov, Uniaxial anisotropy and low-temperature antiferromagnetism of Mn_2BO_4 single crystal, J. Magn. Magn. Mater. 393 (2015) 316-324. https://doi.org/10.1016/j.jmmm.2015.05.081

[24] A. Utzolino and K. Bluhm, New Insights into the Stabilization of the Hulsite Structure During Crystal Structure Determination of $MnII_2MnIII(BO_3)O_2$ and $MnIISrMnIII(BO_3)O_2$, Zeitschrift für Naturforschung B 51 (1996) 1433-1438. https://doi.org/10.1515/znb-1996-1012

[25] J.C. Fernandes, F.S. Sarrat, R.B. Guimaraes, R.S. Freitas, M.A. Continentino, A.C. Doriguetto, and J. Dumas, Structure and magnetism of $MnMgB_2O_5$ and $Mn_2B_2O_5$, Phys. Rev. B 67 (2003) 104413.https://doi.org/10.1103/PhysRevB.67.104413

[26] R.E. Newnham, R.P. Santoro, P.F. Seal, and G.R. Stallings, Antiferromagnetism in $Mn_3B_2O_6$, $Co_3B_2O_6$, and $Ni_3B_2O_6$, physica status solidi (b) 16 (1966) K17-K19. https://doi.org/10.1002/pssb.19660160140

[27] T. Kawano, H. Morito, and H. Yamane, Synthesis and characterization of manganese and cobalt pyroborates: $M_2B_2O_5$ (M= Mn, Co), Solid state sciences 12 (2010) 1419-1421. https://doi.org/10.1016/j.solidstatesciences.2010.05.021

[28] N.B. Ivanova, A.D. Vasil'ev, D.A. Velikanov, N.V. Kazak, S.G. Ovchinnikov, G.A. Petrakovskiĭ, and V.V. Rudenko, Magnetic and electrical properties of cobalt oxyborate Co_3BO_5, Phys. Solid State 49 (2007) 651-653. https://doi.org/10.1134/S1063783407040087

[29] J.L.C. Rowsell and L.F. Nazar, Synthesis, structure, and solid-state electrochemical properties of Cr_3BO_6: a new chromium (III) borate with the norbergite structure, J. Mater. Chem. 11 (2001) 3228-3233. 10.1039/B100707F

[30] K. Kudo, T. Noji, and Y. Koike, Antiferromagnetic ordering in single-crystal $Cu_3B_2O_6$, J. Phys. Soc. Jpn. 70 (2001) 935-938. https://doi.org/10.1143/JPSJ.70.935

[31] E.M. Carnicom, K. Górnicka, T. Klimczuk, and R.J. Cava, The homometallic warwickite V_2OBO_3, Journal of Solid State Chemistry 265 (2018) 319-325. https://doi.org/10.1016/j.jssc.2018.06.021

[32] H. Hagiwara, H. Sato, M. Iwaki, Y. Narumi, and K. Kindo, Quantum magnetism of perfect spin tetrahedra in $Co_4B_6O_{13}$, Phys. Rev. B 80 (2009) 014424. https://doi.org/10.1103/PhysRevB.80.014424

[33] A. Utzolino and K. Bluhm, Synthesis and Crystal Structure of Cobalt Containing Borate Oxides: $Co_{1.5}Ti_{0.5}(BO_3)O$ and $Co_{1.5}Zr_{0.5}(BO_3)O$, Zeitschrift für Naturforschung B 50 (1995) 1653-1657. https://doi.org/10.1515/znb-1995-1111

[34] See Supplemental Material at [URL] for "$Co_{5/3}Nb_{1/3}BO_4$: a new cobalt oxyborate with a complex magnetic structure".

[35] G.M. Sheldrick, A short history of SHELX, Acta Cryst. A 64 (2008) 112-122. https://doi.org/10.1107/S0108767307043930

[36] G.M. Sheldrick, SHELXS and SHELXL97, Program for Crystal Structure Refinement, University of Göttingen, Germany (1997).

[37] N.V. Kazak, M.S. Platunov, Y.V. Knyazev, N.B. Ivanova, Y.V. Zubavichus, A.A. Veligzhanin, and J. Bartolome, Crystal and local atomic structure of $MgFeBO_4$, $Mg_{0.5}Co_{0.}$

$_5$FeBO$_4$ and CoFeBO$_4$: Effects of Co substitution, Phys. Status Solidi (b) 252 (2015) 2245-2258. https://doi.org/10.1002/pssb.201552143

[38] N.E. Brese and M. O'keeffe, Bond-valence parameters for solids, Acta Cryst. B 47 (1991) 192-197. https://doi.org/10.1107/S0108768190011041

[39] J.J. Capponi, Jj Chenavas, and J.C. Joubert, Sur de nouveaux borates mixtes des métaux de transition isotypes de la warwickite, J. Solid State Chem. 7 (1973): 49-54. https://doi.org/10.1016/0022-4596(73)90120-5

[40] R.D. Shannon, Revised effective ionic radii and systematic studies of interatomic distances in halides and chalcogenides, Acta Crystallogr. Sect. A 32 (1976) 751. https://doi.org/10.1107/S0567739476001551

[41] N.V. Kazak, N.A. Belskaya, E.M. Moshkina, L.N. Bezmaternykh, A.D. Vasiliev, S.N. Sofronova, and S.G. Ovchinnikov, Antiferromagnetism of the cation-ordered warwickite system $Mn_{2-x}Mg_xBO_4$ (x= 0.5, 0.6 and 0.7), J. Magn. Magn. Mater. 507 (2020) 166820. https://doi.org/10.1016/j.jmmm.2020.166820

[42] N.V. Kazak, M.S. Platunov, Y.V. Knyazev, E.M. Moshkina, S.Y. Gavrilkin, O.A. Bayukov, and S.G. Ovchinnikov, Fe-induced enhancement of antiferromagnetic spin correlations in $Mn_{2-x}Fe_xBO_4$, J. Magn. Magn. Mater. 452 (2018) 90-99. https://doi.org/10.1016/j.jmmm.2017.12.037

[43] A. Arauzo, N.V. Kazak, N.B. Ivanova, M.S. Platunov, Y.V. Knyazev, O.A. Bayukov, and J. Bartolomé, Spin-glass behavior in single crystals of hetero-metallic magnetic warwickites MgFeBO$_4$, $Mg_{0.5}Co_{0.5}FeBO_4$, and CoFeBO$_4$, J. Magn. Magn. Mater. 392 (2015) 114-125. https://doi.org/10.1016/j.jmmm.2015.05.006

[44] A. Apostolov, M. Mikhov, and P. Tcholakov, Magnetic properties of boron ferrites FeBMeO$_4$, Phys. Status Solidi 56 (1979) K33-K36.

[45] N.V. Kazak, M.S. Platunov, Yu.V. Knyazev, M.S. Molokeev, M.V. Gorev, S.G. Ovchinnikov, Z.V. Pchelkina, V.V. Gapontsev, S.V. Streltsov, J. Bartolomé, A. Arauzo, V.V. Yumashev, S.Yu. Gavrilkin, F. Wilhelm, A. Rogalev, Spin state crossover in Co_3BO_5, preprint (2020) 2009.05725.

[46] N.V. Kazak, M.S. Platunov, N.B. Ivanova, Yu.V. Knyazev, L.N. Bezmaternykh, E.V. Eremin, A.D. Vasil'ev, Crystal structure and magnetization of a $Co_3B_2O_6$ single crystal, JETP 117 (2013) 94-107. https://doi.org/10.1134/S1063776113060186

[47] T. Yang, Y. Wang, D. Yang, G. Li, and J. Lin, Field-induced spin-flop-like metamagnetism in α-CoB_4O_7, Solid State Sciences 19 (2013) 32-35. https://doi.org/10.1016/j.solidstatesciences.2013.02.014

[48] W. Gou, Zh. He, M. Yang, W. Zhang, and W. Cheng, Synthesis and magnetic properties of a new borophosphate $SrCo_2BPO_7$ with a four-column ribbon structure, Inorg. Chem. 52 (2013) 2492-2496. https://doi.org/10.1021/ic3023979

[49] N.B. Ivanova, N.V. Kazak, Y.V. Knyazev, D.A. Velikanov, L.N. Bezmaternykh, S.G. Ovchinnikov, and G.S. Patrin, Crystal structure and magnetic anisotropy of ludwigite $Co_2FeO_2BO_3$, JETP 113 (2011) 1015-1024. https://doi.org/10.1134/S1063776111140172